# Policy, Economics, Management & Transport







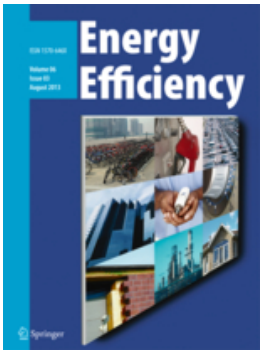


## Energy Efficiency

Editor-in-Chief: Paolo **Bertoldi**

ISSN: 1570-646X (print version)
ISSN: 1570-6478 (electronic version)

Journal no. 12053





### Editor-in-Chief

**Paolo Bertoldi**

Ispra, Italy

e-mail: paolo-bertoldi@libero.it

### Associate Editors

**K. Ehrhardt-Martinez** (Behaviour), *Navigant, Boulder, USA*

**M. Filippini** (Economics of Energy Efficiency) *ETH Zurich and University of Lugano, Switzerland*

**B. Karlin** (Behaviour), *See Change Institute, Venice, USA;*

**M. Kopsakangas-Savolainen** (Economics of Energy Efficiency) *Finnish Environment Institute, Oulu, Finland*

**D. Ürge-Vorsatz** (Energy Efficiency in Buildings) *Central European University, Budapest, Hungary*

**E. Worrell** (Energy Efficiency in Industry), *Utrecht University, The Netherlands*

### Editorial Board

FURTHER LINKS

CNN interview with Marilyn Brown

READ THIS JOURNAL ON SPRINGERLINK

Online First Articles

All Volumes & Issues

Free Access: Special Issue

FOR AUTHORS AND EDITORS

2018 Impact Factor **1.961**

Aims and Scope

Submit Online

Open Choice - Your Way to Open Access

Instructions for Authors Part I

Instructions for Authors Part II

SERVICES FOR THE JOURNAL

Contacts

Download Product Flyer

Shipping Dates

Article Reprints

Bulk Orders

ALERTS FOR THIS JOURNAL

Get the table of contents of every new issue published in Energy Efficiency.

LOGIN

Please send me information on new Springer publications in Energy Policy, Economics and Management.

ADDITIONAL INFORMATION

European Council for an Energy Efficient...

Become a Facebook fan of ECEEE!

RELATED BOOKS - SERIES - JOURNALS


Journal

Energy, Sustainability and Society

**Editor»** Editor-in-Chief: Daniela **Thrän**

BACK NEXT 1/10

Skip to main content

Energy Efficiency
All Volumes & Issues
ISSN: 1570-646X (Print) 1570-6478 (Online)

## In this issue (13 articles)

Support

Energy Efficiency (2018) 11:955–974
https://doi.org/10.1007/s12053-017-9603-7

ORIGINAL ARTICLE

# Assessing the energy saving potential of anidolic system in the tropics

**Floriberta Binarti** · **Prasasto Satwiko**

Received: 30 January 2016 / Accepted: 7 December 2017 / Published online: 24 January 2018


**Abstract** Employing the edge-ray principle, the anidolic system (AS) has been proven as a promising daylighting solution for various climates. However, studies on the thermal performance of an AS are still rare. Because of the dominant contribution of the space-cooling load to building energy consumption at the operational stage in hot climates, knowledge of the impact of AS application on the space-cooling load is important. This study assessed the energy-saving potential of AS in the tropics by measuring the daylight level and distribution, as well as the solar heat gain, based on Radiance and EnergyPlus simulations using weather files of two locations in the tropics—Yogyakarta and Singapore. Monitoring data of a full-scale, unoccupied test building was acquired to validate the Radiance simulations and EnergyPlus models. A comparison between the energy-saving potential for lighting and cooling of AS and conventional aperture models showed that the application of AS in the tropics benefits the daylighting performance (DF ≥ 3% and horizontal distribution 51–70%), but still produces higher solar heat gains (44–437% higher than those of clerestory only). Narrow anidolic collectors with medium angular spread (45°–52°) and maximum clerestory height equipped with internal shelves can be applied to produce lower solar heat gain or indoor air temperature (2%) with sufficient daylight levels (≥ 2%) and an increased in horizontal illuminance distribution (> 57%).

**Keywords** Anidolic system · Daylight factor · Indoor illuminance distribution · Solar heat gain · Tropics

**Nomenclature**

| | |
|---|---|
| AS | anidolic system |
| $A_{win}$ | window area |
| CL | clerestory |
| Cx_Ay_wz | y-m-wide, z-degree-angular spread anidolic collector installed on a x-m-height clerestory |
| DF | daylight factor |
| dT | temperature difference |
| ECHTC | external convective heat transfer coefficient |
| eAd | Adaptive Algorithm for external convective heat transfer coefficient |
| eDO | DOE-2 for external convective heat transfer coefficient |
| eTA | TARP for external convective heat transfer coefficient |
| eMo | MoWiTT for external convective heat transfer coefficient |
| $E_i$ | indoor illuminance |
| $E_o$ | outdoor illuminance |
| $\varepsilon_{room}$ | indoor surface emissivity |
| $\varepsilon_{win}$ | interior window surface emissivity |
| $F_{win\text{-}room}$ | view factor from the window to the other surfaces of the room |
| HS | horizontal shading |

F. Binarti (✉) · P. Satwiko
Department of Architecture, Atma Jaya Yogyakarta University, Jl. Babarsari 44, Yogyakarta 55281, Indonesia
e-mail: flo.binarti@gmail.com
e-mail: binarti@mail.uajy.ac.id

| | |
|---|---|
| ICHTC | internal convective heat transfer coefficient |
| iA | Adaptive Algorithm for internal convective heat transfer coefficient |
| iT | TARP for internal convective heat transfer coefficient |
| IS WS | intermediate sky with the sun |
| $Q_{IR}$ | net heat transfer from the window to the room surfaces |
| $T_i$ | indoor air temperature |
| $T_o$ | outdoor (ambient) air temperature |
| WFR | window to floor area ratio |
| x_AS | anidolic system installed on x-m-wide room |
| x_Ay | x-m-wide anidolic system installed on y-m-wide room |

## Introduction

Due to rapid urban growth and climate change, it takes great effort to create a pleasant, healthy, and energy-efficient indoor space in an urban area. An aperture is a building element that plays an important role in achieving such a pleasant, healthy, and energy-efficient indoor space (Erell et al. 2014; Michael and Heracleous 2016). Apertures can impact the energy use of a building through four basic mechanisms—thermal heat transfer, solar heat gain, air leakage, and daylighting (ASHRAE 2013). Usually, the conductive heat transfer through fenestration is higher than that through the opaque building envelope because the thermal transmittance of glass, the most common aperture material, is usually higher than that of the opaque material (ASHRAE 2013). In the tropics, the solar heat gain that enters the space only through a transparent material becomes the main contributor to heat transfer (Sunaga et al. 2008; ASHRAE 2013). Hence, in air-conditioned buildings, although the daylight aperture functions more as a view window and/or daylight opening, high performance apertures should minimize their thermal impact in creating a thermally comfortable space while decreasing the energy for cooling to enhance the occupant productivity.

An anidolic system (AS) is a kind of daylight aperture that works based on the edge-ray principle. Renowned as a highly efficient daylight aperture, several studies show that an AS can achieve outstanding daylighting performance (Scartezzini and Courret 2002; Wittkopf 2006; Binarti and Satwiko 2015). The AS was initially intended to improve the daylighting performance of inner rooms in temperate climates under overcast sky conditions, by efficiently collecting and redistributing the diffuse component of daylight (Scartezzini and Courret 2002). Basically, anidolic devices consist of a parabolic collector and a light diffuser. The parabolic form is aimed to capture zenithal light at a wide range of time. Although its effective light capture duration is more limited (Binarti and Satwiko 2016) than the ability of adaptive shading facade system in redirecting natural light into the interior (Michael et al. 2017), anidolic system still can be classified as an advanced passive daylighting system.

The zenithal anidolic collector is the first design of AS, and comprises two compound parabolic concentrators (CPC)—an exterior collector and an internal daylight beam projector installed in the other direction (Kleindienst 2006). In Lausanne, an anidolic integrated ceiling (AIC) was designed to meet the requirements imposed by building integration constraints and user acceptance (Scartezzini and Courret 2002). Despite the limited application of AS due to a lack of planning tools and guidelines for architects and engineers (Wittkopf et al. 2010), several studies on AS daylighting performance in various climates have been conducted.

Kleindienst (2006) studied the factors influencing the daylighting performance of AS and classified them into two categories. The amount of light captured from the zenithal sky depends on the size and angular range of the exterior collector. On the other hand, the size, height, and angular spread of the interior parabolic pair belong to the second category, which determines the daylight factor (DF) distribution. Linhart et al. (2010) conducted a parametric study on AIC performance in Singapore. Based on Photopia simulations of the AIC daylighting performance under a virtual sky dome, representing Singapore's sky conditions, they identified four main factors influencing the system efficiency as follows: coating reflectivity (31%), duct length (24%), external shading (18%), and duct width (5%). An extremely thin silver layer was selected to provide the highest reflectivity (98%) (Linhart et al. 2010). However, the price of this coating material is still high for developing countries. Stainless steel (reflectance: 90%) has been proven as an appropriate collector material in previous studies in Thonburi, Thailand (latitude 13°57' N and longitude 100°44′ E) (Praditwattanakit et al. 2013) and Yogyakarta, Indonesia (latitude 7°49' S and longitude 110°21′ E)

(Binarti and Satwiko 2016). Furthermore, seven variants of the virtual AIC collectors with 50-cm-high apertures were tested to develop a method for predicting the luminous intensity distribution curves (LIDC) (Wittkopf et al. 2010). Employing a forward ray-tracing simulation technique, LIDC was derived as a function of 2D flux, angular spread, and horizontal offset angle. The experiment results demonstrated that a 1-m-wide parabolic collector with an entry aperture of 90° performed the best. Additional deconcentrators improved the symmetry of the spread, but they could not produce high light flux due to the decrease in the aperture size. Although the collectors vary in width, the impact of the collector width on the daylighting performance was not evaluated. In Malaysia, daylighting performance of ADS has been examined based on the collector orientation (Roshan et al. 2013).

Unfortunately, all studies on AS mentioned above discussed the daylighting aspect only. Studies on the thermal performance of AS are rare. In the tropics, which receive high intensity solar radiation, mainly falling on a horizontal plane, the zenithal glazing of the anidolic collector may receive high solar transmission during daytime, which further increases building energy cooling (Al-Obaidi et al. 2014). Smaller glazing inclination receives higher amounts of incident solar radiation, while a larger glazing area receives higher amounts of incident solar radiation. For tropical climates, a daylight aperture with low solar heat gain would save a significant amount of energy (Binarti 2009), since tropical buildings generally consume 60% of the total energy at the operational stage for air conditioning (Prasetyo and Kusumarini 2016). Therefore, a compromise between low cooling load and high daylighting performance becomes the main issue for energy-optimized aperture design in the tropics.

A long-term monitoring and simulation study of an east-facing AS with a 40-cm-high opening in a 3-m-wide room of a tropical urban house in Yogyakarta shows that increasing the daylighting as well as the thermal performance of AS in tropical buildings are possible (Binarti and Satwiko 2015). Solar radiation transmitted by the narrow zenithal glazing of the east-facing AS does not increase in the indoor air temperature. However, application of AS in wide (> 6 m) rooms requires larger openings that potentially increase the solar heat gain. Thus, to obtain an energy-efficient AS, identifying the energy performance of the AS in the tropics is necessary. In this experimental study, the energy performance of the AS in the tropics was identified by comparing the simulated daylighting performance and thermal performance of AS with those of other aperture (conventional) models. Field measurements were used to validate the daylighting simulation results and determine the appropriate models used in building energy simulations.

## Methods

### Parametric study

To obtain the optimum energy performance of AS, 3D–models of the anidolic collector, varying in width/angular spread, were constructed. The width of a collector was defined by the aperture height and three variations of angular spread. These variations are chosen based on the previous studies (Kleindienst 2006; Wittkopf et al. 2010; ASHRAE 2013; Binarti and Satwiko 2016) as discussed in the Introduction. The aperture area corresponds to approximately 9.5% of the floor area (window to floor area ratio or WFR) with 2.1 m of sill height. This value is close to the minimum value recommended by LEED (2009), 10%, whereas a previous study (Binarti and Satwiko 2016) discovered that the application of AS in the tropics demands less than 10% of the WFR. Each collector consists of parabolic stainless steel (light reflectance: 90%) and a single clear glass (light transmittance: 90%). All models were equipped with a ceiling integrated light diffuser (light reflectance: 90%).

Each collector was installed in a single building with a single zone that varies in width and height (Table 1 and Fig. 1). These variations represent common classroom/open-plan office widths and are selected to observe the optimum room width for AS application. Room models with the same length (6 m), interior reflectance, and room length were constructed. The interior reflectances refer to the IESNA (2000) maximum recommendations, i.e., 90% for the ceiling reflectance, 75% for the wall reflectance, and 50% for the floor reflectance.

To investigate the energy saving potential of AS with different collector widths, the daylighting and thermal performance of nine models in Fig. 1 were simulated. There are two main steps in the simulation study. First, the Radiance based software was employed to calculate the indoor illuminance, daylight factor (DF), and the distribution. EnergyPlus was used to predict the thermal

**Table 1** Variant models of AS

| Room width (m) | Room height (m) | Aperture area ($cm^2$) | Aperture head height (m) | Collector/shading angular spread/tilt angle | Collector/shading width (cm) | Code |
|---|---|---|---|---|---|---|
| 6 | 3 | 60 × 560 | 2.8 | $37^o$ | 48.0 | 6_A048 |
| | | | | $47^o$ | 60.0 | 6_A060 |
| | | | | $52^o$ | 72.0 | 6_A072 |
| | | | | $30^0$ | 60.0 | 6_H |
| 8 | 3.2 | 80 × 560 | 2.9 | $45^o$ | 85.3 | 8_A085 |
| | | | | $55^o$ | 106.7 | 8_A107 |
| | | | | $60^o$ | 128.0 | 8_A128 |
| | | | | $30^0$ | 80.0 | 8_H |
| 10 | 3.5 | 100 × 560 | 3.1 | $57^o$ | 133.3 | 10_A133 |
| | | | | $60^o$ | 166.7 | 10_A167 |
| | | | | $67^o$ | 200.0 | 10_A200 |
| | | | | $30^0$ | 100.0 | 10_H |

performance (solar heat gain and indoor air temperature) in the second step. The energy-saving potential of AS was assessed by comparing the daylighting performance and solar heat gain of a building equipped with AS with those of the same building model equipped with clerestory—to represent the basic aperture—and with 30°-tilted horizontal shading—to represent the conventional shading in tropical regions (Fig. 2 and Table 1). This study selects Yogyakarta and Singapore as the locations. Yogyakarta represents a tropical region in the southern hemisphere at 110°26′ E, 7°32’ S, while Singapore represents a tropical region in the northern hemisphere (1.4° N, 104° E). Additionally, several previous studies on AS have been carried out in these cities.

## Anidolic collector model in radiance

Radiance (Ward 2002) has been widely used to predict daylighting performance, based on the backward ray-tracing method. Besides the capability of the algorithm in calculating daylighting performance (Reinhart and Andersen 2006; McNeil and Lee 2012), a sky luminance model is essential to test the accuracy of daylighting simulations. Radiance, plugged in Ecotect (Marsch 2005), provides four sky luminance model options—sunny sky (CIE clear sky), intermediate sky, cloudy sky (CIE overcast sky), and uniform sky.

The sky type in warm climates is often described as a predominantly overcast sky (Sunaga et al. 2008).

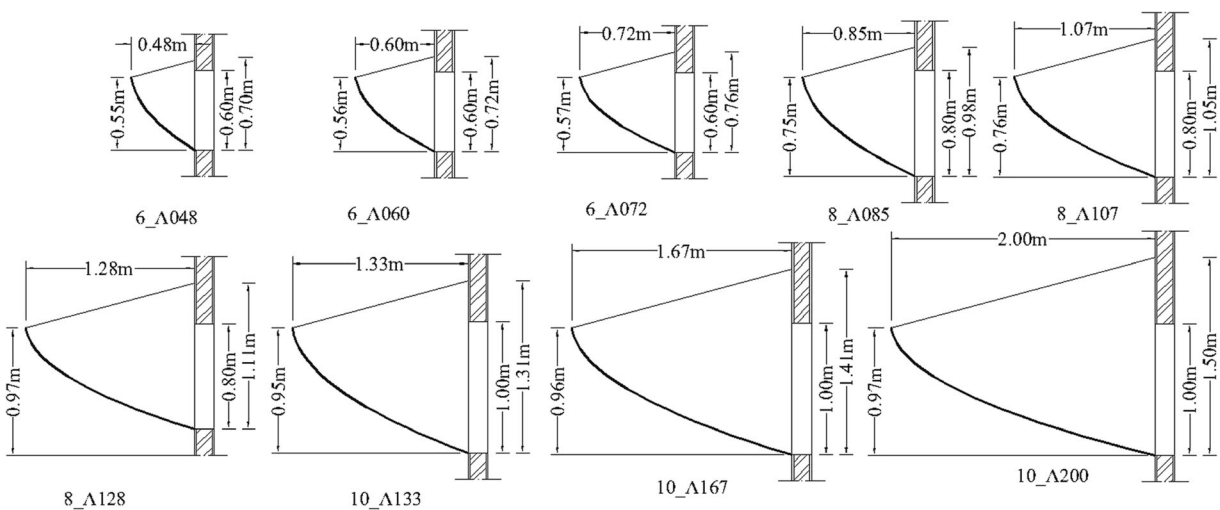


**Fig. 1** Anidolic collector models

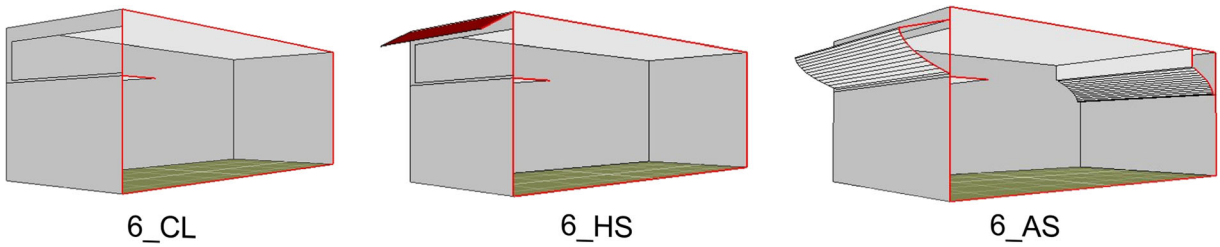


**Fig. 2** From left to right: model with clerestory only (6_CL), model with horizontal shading (6_HS), and model with anidolic system (6_AS)

However, daylight measurements in South East Asia have shown different conditions. A study on the tropical sky luminance distribution conducted in Bangkok (Chirarattananon and Chaiwiwatworakul 2007) concluded that partly cloudy and clear skies with 30% overcast sky dominated the local sky occurrence in a year. Based on measurements of the cloud cover ratio, Rahim and Mulyadi (2004) suggested a luminance distribution of 15.32% clear sky, 69.80% intermediate sky, and 14.88% overcast sky for Makassar, Indonesia (119° E, 5.8° N).

Calculation of the DF has been a dominant method used to analyze daylighting performance over several decades. It describes the ratio of the indoor illuminance at a specific point in a space ($E_i$) to the simultaneous unobstructed outdoor illuminance ($E_o$). Radiance (plugged in Ecotect) adopts the BRE split flux method to calculate the DF (Marsch 2005). The DF calculation uses an overcast sky representing the worst sky conditions, exactly at noon in mid-winter. Because the DF is climate- and orientation-independent, it cannot measure the climate-, time-, or orientation-based aperture performance. However, the DF can be used to measure the daylighting performance, which is based on the geometric and optical properties. The optimum DF for working (including reading and writing in a classroom/office) is 2%.

Since an even indoor illuminance distribution seems brighter to human eyes than an uneven one (Aizlewood 1993), this study employs the distribution of the DF as another daylighting parameter. The indoor illuminance or DF distribution can be determined by dividing the minimum DF or indoor illuminance by the average DF or indoor illuminance. Pritchard (1986) suggested 75% of the indoor illuminance or DF distribution as the minimum indoor illuminance or DF distribution. To give information about the illuminance related to time, location, and aperture orientation, the indoor illuminance was simulated under an intermediate sky.

To produce accurate simulation results, all simulations were set in four indirect reflections, very detailed model, high lighting variability, and high image quality. Unfortunately, backward ray-tracing in Radiance cannot handle intense, direct sunlight on curved reflectors well. To solve this problem, Compagnon suggested more resolution in modeling the curve for simulations of an AS under diffuse skies (in Kleindienst 2006). This study constructed anidolic collector models from 5-cm-wide surfaces arranged in parallel, forming a quite high resolution segmented curve. In comparison to the total curve circumferences (which vary), 5 cm in width can be considered as quite narrow (high).

## Anidolic collector model in EnergyPlus

This study used the EnergyPlus engine (Crawley et al. 2013) to analyze the thermal performance and energy consumption of the model. EnergyPlus is one of building energy simulation programs in use today. It employs the zone heat balance method, including the surface and zone air heat balance for thermal load calculations (UIUC and LBNL 2015). Several studies on the effects of building envelope (Hachem et al. 2011) and fenestration systems (Huang et al. 2014; Singh et al. 2015; Goia 2016) on the solar potential and energy performance have relied on the accuracy of EnergyPlus.

For various apertures with 6-mm-thick clear single glass in a single building, solar heat gain is the most important factor that can be modified by apertures (ASHRAE 2013). EnergyPlus uses a complete radiative network model to represent a radiative exchange between surfaces. The solar heat gain is quantified from the solar radiation transmitted through and absorbed by the window glazing. Solar radiation on the window exterior surface is a sum of direct solar radiation, sky diffuse radiation, and ground reflected diffuse radiation. The Perez solar radiation model is employed to split the global solar radiation into direct normal and diffuse

horizontal components. The sky diffuse radiance distribution is assumed to be anisotropic (UIUC and LBNL 2015). The comparative (Loutsenhiser et al. 2007) and empirical (Loutsenhiser et al. 2008) validation in solar heat gain calculation has proven the accuracy of the Perez solar radiation model in calculating the solar irradiance on the glazing window and the solar heat gain entering a solar selective glazing, respectively.

In EnergyPlus, the net heat transfer from the window to the room surfaces ($Q_{IR}$) is described in Eq. 1 (Zhu et al. 2012). EnergyPlus uses an approximate view factor for the radiative heat transfer calculation. Despite the reduction in accuracy from the accuracy of the exact view factor, verification of the radiative heat transfer conducted by Ellis (2003) shows that the errors of the approximate view factor are small compared to exact view factor.

$$Q_{IR} = \frac{\sigma\left(T_{win}^4 - T_i^4\right)}{\frac{1-\varepsilon_{win}}{\varepsilon_{win}A_{win}} + \frac{1}{A_{win}F_{win\rightarrow room}} + \frac{1-\varepsilon_{room}}{\varepsilon_{win}A_{win}}} \quad (1)$$

Convective heat transfer is a heat transfer mode, which determines the window surface temperature. EnergyPlus provides several models to calculate the exterior and interior convective heat transfer coefficient (ECHTC and ICHTC). ECHTC depends on the wind speed and direction, surface orientation and slope angle, terrain type, sheltering by surrounding, surface to air temperature difference, surface texture, size, and aspect ratio (Mirsadeghi et al. 2013).

## Validation study

In this study, a validation study is intended to ensure which convective heat transfer model of EnergyPlus conforms to the case study and to observe the limitations of Radiance in predicting the daylighting performance. A 2.5-m-long, 6-m-wide building was built for the test facility located on a site relatively free of external obstruction in Yogyakarta (7°49′24.55” S and 110°24′ 31.56″ E) for the purpose of empirical validation. No mechanical ventilation or air conditioner was installed. Only wind or buoyancy-driven natural ventilation worked across two small openings on the west wall and two small openings on the east wall. Material properties of the test facility are explained in Table 2. North-facing clerestory (see Fig. 3) was installed in the facility and monitored on May 8, 9, 11, 13, 15, 27–30, and June 3 from 8 a.m. to 4 p.m. At first, a clerestory without shading was installed as the base model for May 8 to 9, 11, 13, and 15. From May 27 to 30 and on June 3, a 73-cm-wide AS replaced the clerestory glazing for the second monitoring.

The monitoring data were acquired from the following:

- Two Hobo Dataloggers U12–012 for continuous measurement of the indoor air temperature, relative humidity, and indoor illuminance were placed inside the building as described at points A, B, and C in Fig. 3. The accuracy is ± 0.35 °C for the temperature sensor and ± 2.5% for the humidity sensor.
- Two 4-in-1 Environment Testers LM-8000 were used for hourly measurement of the outdoor relative humidity and wind speed. One of them was exposed to solar radiation and the other was located under the shadow at point D in Fig. 3. The accuracy is + 1% or +1 °C for the temperature sensor, and 4% or + 1.2% for the humidity sensor, ± 5% for the light sensor, ± 3% for wind speeds less than 20 ms and ± 4% for wind speeds greater than 20 ms.
- A Power Meter SP2065 for global solar radiation at point D.
- Two Hobo Dataloggers UA 002-08 for continuous measurement of the outdoor air temperature and illuminance were located outside the building, in which one was exposed to solar radiation and the other was under a shadow at point E in Fig. 3. The accuracy is ± 0.47 °C for the temperature sensor and ± 2.5% for the humidity sensor.

The test facility was constructed as an unequipped and naturally ventilated zone using Design Builder for the thermal simulations and Ecotect for the daylighting simulations. To observe how closely Radiance predicts the daylighting performance, author-selected sky luminance models, which can simulate the $E_i$ most closely to the real ones, were chosen.

Since validation of EnergyPlus is more intended to identify the most suitable interior convective heat transfer coefficient (ICHTC or i) and exterior convective heat transfer coefficient (ECHTC or e) models, this study selected Adaptive Algorithm and TARP for the ICHTC, and the ECHTC, DOE-2, and MoWiTT for the ECHTC. An adaptive Algorithm was selected for the most comprehensive models (UIUC and LBNL 2015), while TARP is the default ICHTC model. The TARP ECHTC

**Table 2** Material properties

| Layer number | Material | Thickness (mm) | Thermal conductivity (W/(m.K)) | Density (kg/m$^3$) | Specific heat (J/(kg K)) |
|---|---|---|---|---|---|
| Wall: brickwork single leaf construction light plaster | | | | | |
| 1 | Cement/plaster/mortar | 10 | 0.72 | 1760 | 840 |
| 2 | Concrete block (lightweight) | 130 | 0.19 | 600 | 1000 |
| 3 | Plaster (lightweight) | 10 | 0.16 | 1000 | 600 |
| Floor: combined ground floor, uninsulated, lightweight | | | | | |
| 1 | Floor screed | 70 | 0.41 | 1200 | 840 |
| 2 | Cast concrete | 100 | 1.13 | 1000 | 2000 |
| Horizontal shading | | | | | |
| Cast concrete lightweight | | 800 | 0.38 | 1200 | 1000 |
| | | | Thermal absorptance | Solar absorptance | Visible absorptance |
| | | | 0.9 | 0.6 | 0.6 |
| Roof: combined flat roof, uninsulated, lightweight | | | | | |
| 1 | Asphalt | 19 | 0.70 | 2100 | 1000 |
| 2 | Air gap | 100 | Resistance: 0.18 m$^2$.K/W | | |
| 3 | Plasterboard | 13 | 0.25 | 2800 | 896 |
| Anidolic system: | | | | | |
| | Stainless steel | 1.5 | 17.00 | 460 | 7900 |
| | Gypsum board | 13 | 0.25 | 900 | 1000 |
| | Single clear glass | 6 | 0.90 | | |
| | | Visible transmittane | Solar transmittance | Outside emissivity | Inside emissivity |
| | | 0.881 | 0.775 | 0.840 | 0.840 |

model accounts for the terrain roughness, surface orientation, and the difference between the surface and zone air temperatures (Zhu et al. 2012). DOE-2 is the default ECHTC model that calculates the convective coefficient for very smooth surfaces like window glazing. This model considers different terrain types, but it does not consider variations in the sheltering effects of surrounding buildings. MoWiTT was tested for the ECHTC model because it is suitable for application to window glass in low-rise buildings, although it does not consider sheltering effects and terrain types.

## Simulation set-up

After Radiance was validated and the ECHTC and ICHTC models in EnergyPlus were selected, the next step was to define the simulation set-up for all variations described in Table 1. Radiance was employed to predict the DF, indoor illuminance, and its distribution, while EnergyPlus was used to compute the solar heat gain and the indoor air temperature in the building models using the climate data of Yogyakarta and Singapore. Material properties of all models are displayed in Table 2. Aside from DF simulations (under the overcast sky), simulations of the indoor illuminance under the intermediate sky with the sun (IS WS) were performed twice for each model, in each location and aperture orientation to represent the highest and lowest solar angle of incidence. There are two variations in orientation for all aperture models in each location, which are selected based on previous studies. Apertures in the southern hemisphere are oriented to the North and East as the best orientation (Binarti and Satwiko 2016), while apertures in the northern hemisphere are oriented to the South and East as the best orientation (Linhart et al. 2010; Roshan et al. 2013).

For the EnergyPlus simulations, the 3D–models were created using DesignBuilder (Tindale and Potter 2014).

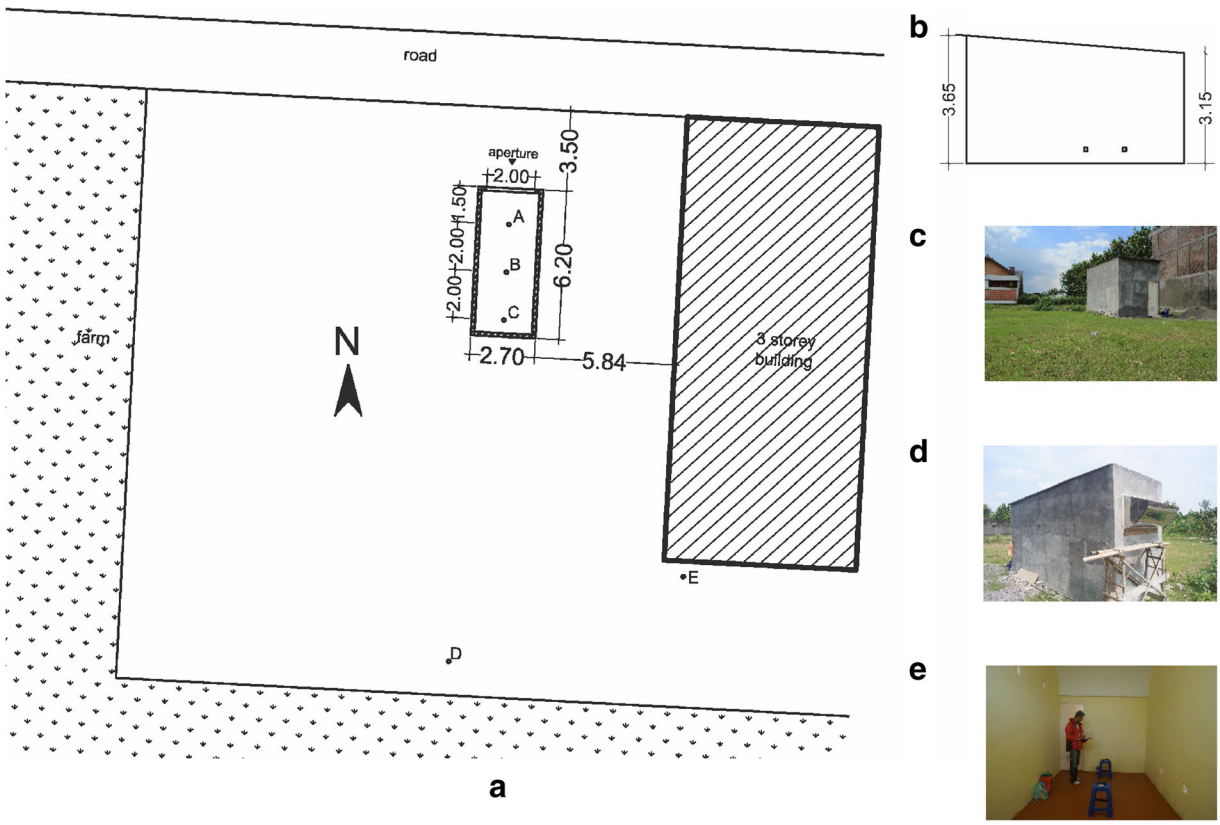


**Fig. 3** **a** Location of the test facility and measurement points: A-B-C: inside the building; D: exposed to direct solar radiation/sunshine; E: under shadow. **b** The section of the test facility. **c** The test facility with the surrounding environment. **d** The test facility equipped with anidolic system. **e** The test facility's interior

Basically, there are three aperture models, which should be treated differently. The reference model is a simple building equipped with clerestory. The second model resembles the reference model, equipped with horizontal shading device. An AS-equipped building model is created from two zones—the reference model zone and the collector zone. These zones were further merged into a single zone, i.e., "standard" or the occupied zone. All space models are treated as air-conditioned zones and naturally ventilated zones. Split with no fresh air was selected, as it is commonly applied in small to medium buildings with 2.7 of the Coefficient of Performance (COP) of the Air Conditioner system (SNI 2011). The cooling system was set at 26 °C as the maximum temperature for a thermally comfortable working space in the tropics (SNI 2011). The infiltration rate in this zone was scheduled for air conditioning spaces and calculated by EnergyPlus for naturally ventilated spaces with one per hour for the air change rate.

## Results and discussions

### Deviation and discrepancy of the radiance simulations

Most of the simulated indoor illuminance values, which are close to the measured indoor illuminance values, were obtained by using clear sky with the sun. Average discrepancies ranging from 0 to 14% (Table 3 and Fig. 12 in Appendix) show that simulation results agree quite well with measurement results. Simulations on May 5 and 15 for the base model, on May 27–28 for the AS1 model, and on June 10–11 for AS2 were performed under the most suitable sky conditions that varied according to the sky condition at that time. On these days, the ratio of the real indoor illuminance ($E_i$) to the real outdoor illuminance ($E_o$) or DF has the smallest deviations. Under the regular pattern of sky luminance (AS2), the maximum discrepancy is only 11% on June 10 and 10% on June 11. However, large deviations (−473 Lux and −106 Lux) occurred in the distance of

**Table 3** Radiance and EnergyPlus simulation set-up

| | | | |
|---|---|---|---|
| `Radiance | Model location and aperture orientations with simulation dates (Max–Min) | Yogyakarta | North (N):<br>September 22 at 12:00 (IS WS N-22 sep 12:00)—the highest sun's angle of incidence<br>December 21 at 16:00 (IS WS N-21 dec 16:00)—the lowest sun's angle of incidence |
| | | | East (E):<br>October 16 at 11:00 (IS WS N-16 oct 11:00)—the highest sun's angle of incidence<br>June 21 at 16:00 (IS WS N-21 jun 16:00)—the lowest sun's angle of incidence |
| | | Singapore | South (S):<br>March 21 at 12:00 (IS WS N-21 mar 12:00)—the highest sun's angle of incidence<br>June 21 at 16:00 (IS WS N-21 jun 16:00)—the lowest sun's angle of incidence |
| | | | East (E):<br>April 1 at 11:00 (IS WS N-1 apr 11:00)—the highest sun's angle of incidence<br>December 21 at 16:00 (IS WS N-21 dec 16:00)—the lowest sun's angle of incidence |
| EnergyPlus | Site | Exposure to wind | Normal |
| | Activity | Generic office area, no equipments | |
| | Air-conditioned space | AC system | Split no fresh air |
| | | Cooling system COP | 2.7 |
| | | Cooling set point | 26 °C |
| | | Airtightness: model infiltration | Scheduled, constant rate: 1 ac/h |
| | Naturally ventilated space | System | No heating/cooling |
| | | Wind factor | 1 |
| | | Airtightness: model infiltration | Calculated, good, constant rate: 1 ac/h |

1.5 and 5.5 m from the aperture in the base model and on May 15 due to high fluctuations in the ambient illuminance. These indicate that Radiance tends to overestimate the indoor illuminance (from − 0.09 to − 0.14) when the sun altitude is high.

## Deviation and discrepancy of the EnergyPlus models

Comparison between the climate elements of the site and the weather file shows differences in ambient temperature. The average temperature difference (dT) on May 8, 9, 11, 13, and 15 is 4.19, whereas on May 27, 28, 29, 30, and June 3 is 4.15. Tables 4 and 5 display the deviations and discrepancies between the monitoring data and the simulations of the ambient ($T_o$) and indoor air temperature ($T_i$) of the test facility. Deviations and discrepancies between measured dT and EnergyPlus-simulated dT look similar. Similar deviations and discrepancies can be also observed among the results of EnergyPlus models. They show that simulations of EnergyPlus using two models of ICHTC and four models of ECHTC are in good agreement with the monitoring data, especially simulations of the test building equipped with AS that generally have < 10% of the discrepancy. Although discrepancies between simulations of test facility with clerestory are higher, they are still < 20%. A different deviation in $T_i$ only reveals the result of the combinations of TARP and DOE-2 in test facilities equipped with AS. Since model appropriateness was measured by the smallest temperature difference of simulation results to that of monitoring data, and the similarity of the deviations and discrepancies in $T_i$ and $T_o$, the best results are combinations of interior TARP and exterior TARP, and of the interior Adaptive Algorithm and any ECHTC model. This can be understood since TARP considers the terrain roughness (the

**Table 4** Deviations and discrepancies between field measured and simulated Ei

| Models | Date | Real DF–sim DF (deviation of DF) | | | | Real Ei–sim Ei (deviation of Ei) in Lux | | | | (Real Ei–sim Ei)/real Ei (discrepancy of Ei) | | | |
|---|---|---|---|---|---|---|---|---|---|---|---|---|---|
| | | 1.5 | 3.5 | 5.5 | Avg | 1.5 | 3.5 | 5.5 | Avg | 1.5 | 3.5 | 5.5 | Avg |
| Clerestory | 08.05 | 0.04 | 0.04 | 0.02 | 0.03 | 31 | − 64 | − 106 | − 46 | 0.03 | − 0.09 | − 0.22 | − 0.09 |
| | 15.05 | 0.08 | 0.02 | 0.01 | 0.04 | − 473 | − 87 | 12 | − 183 | − 0.35 | − 0.09 | 0.04 | − 0.13 |
| AS1 | 27.05 | 0.03 | 0.03 | 0.02 | 0.02 | 46 | − 13 | − 35 | − 1 | 0.02 | − 0.11 | − 0.08 | − 0.06 |
| | 28.05 | 0.04 | 0.04 | 0.03 | 0.03 | − 26 | − 46 | − 46 | − 42 | − 0.12 | − 0.18 | − 0.11 | − 0.14 |
| AS2 | 10.06 | 0.02 | 0.02 | 0.01 | 0.02 | 52 | 3 | − 19 | 12 | 0.11 | − 0.02 | − 0.09 | 0.00 |
| | 11.06 | 0.03 | 0.04 | 0.02 | 0.03 | 63 | 21 | − 4 | 27 | 0.10 | − 0.09 | − 0.12 | − 0.04 |

dense surrounding of the test facility), surface orientation, and the difference between the surface and zone air temperatures (Zhu et al. 2012) (Tables 5 and 6).

Calculations of the solar heat gain inside the test building equipped with AS using various ECHTC and ICHTC models (see Fig. 4) demonstrate rather different results. Various combinations of ECHTC and ICHTC models do not create any differences in calculations of the solar heat gain for May 8, 9, and 11. On May 13 and 15, different ICHTC and ECHTC models result in significant differences in the solar heat gain calculations. Figure 4 shows that two different results appeared on May 13 and 15, which can be further classified into two groups of combinations of the ECHTC and ICHTC. The first group of the ECHTC and ICHTC combination is DOE-2–TARP, Adaptive Algorithm–TARP, MoWitt–TARP, TARP–TARP, and TARP–Adaptive Algorithm. The second group is DOE-2–Adaptive Algorithm and TARP–Adaptive Algorithm. Space solar heat gain calculated using Adaptive Algorithm–Adaptive Algorithm has close results to the calculations using the second combination group on May 8, 9, and 11. On May 13 and 15, calculations using the second group of the combination of ECHTC and ICHTC models produces a higher solar heat gain than calculation results using the first combination group of ECHTC and ICHTC models.

The climate data file shows an increase in wind velocity and solar radiation starting from May 11 to May 15. An increase in wind velocity may reduce the space solar heat gain by decreasing the glazing surface temperature and the wind-driven natural ventilation inside the test facility. The first group of the ECHTC and ICHTC combination, which uses TARP as the ICHTC, seems more sensitive to the effect of increasing wind velocity. It proves TARP as a comprehensive natural convection model for the interior surface (Zhu et al. 2012). Based on the validation results of the test facility equipped with AS, the next simulations used interior TARP–exterior TARP.

**Table 5** Deviations and discrepancy between measured and EnergyPlus simulated air (dry bulb) temperature, and thermal difference (dT = To−Ti) outside and inside the base model

| | Average deviation/discrepancy (deg C) of ICHTC-ECHTC model | | | | | | | | |
|---|---|---|---|---|---|---|---|---|---|
| | Real | eDO-iT | eAd-iT | eTA-iT | eMo-iT | eDO-iA | eAd-iA | eTA-iA | eMo-iA |
| Real Ti–sim Ti | | 4.683 | 4.683 | 4.726 | 4.691 | 4.551 | 4.664 | 4.664 | 4.664 |
| Real To–sim To | | 4.733 | 4.733 | 4.733 | 4.733 | 4.733 | 4.733 | 4.733 | 4.733 |
| (Real Ti–sim Ti)/real Ti | | 0.149 | 0.149 | 0.149 | 0.149 | 0.145 | 0.148 | 0.148 | 0.148 |
| (Real To–sim To)/real To | | 0.128 | 0.128 | 0.128 | 0.128 | 0.128 | 0.128 | 0.128 | 0.128 |
| $dT = (T_o - T_i)$ | 4.190 | 4.140 | 4.140 | 4.183 | 4.148 | 4.008 | 4.121 | 4.121 | 4.121 |

*iT* TARP for interior convective heat transfer coefficient; *iA* adaptive algoritm for interior convective heat transfer coefficient; *eDO* DOE-2 for external convective heat transfer coefficient; *eAd* adaptive algorithm for external convective heat transfer coefficient; *eTA* TARP for external convective heat transfer coefficient; *eMo*: MoWitt for external convective heat transfer coefficient

**Table 6** Deviations and discrepancy between measured and EnergyPlus simulated air (dry bulb) temperature, and thermal difference (dT = To − Ti) outside and inside test building equipped with 85-cm-wide AS (AS1)

| | | Average deviation/discrepancy (deg C) of ICHTC-ECHTC model | | | | | | | | |
|---|---|---|---|---|---|---|---|---|---|---|
| | | Real | iT-eD | iT-eA | iT-eT | iT-eM | iA-eD | iA-eA | iA-eT | iA-eM |
| Deviation | Ti | | 2.055 | 3.008 | 3.008 | 3.008 | 2.985 | 2.992 | 2.992 | 2.992 |
| | To | | 3.024 | 3.024 | 3.024 | 3.024 | 3.024 | 3.024 | 3.024 | 3.024 |
| discrepancy | Ti | | 0.066 | 0.098 | 0.098 | 0.098 | 0.097 | 0.097 | 0.097 | 0.097 |
| | To | | 0.084 | 0.084 | 0.084 | 0.084 | 0.084 | 0.084 | 0.084 | 0.084 |
| $dT = (T_o - T_i)$ | | 4.150 | 3.180 | 4.133 | 4.133 | 4.133 | 4.110 | 4.117 | 4.117 | 4.117 |

*iT* TARP for interior convective heat transfer coefficient; *iA* adaptive algorithm for interior convective heat transfer coefficient; *eD* DOE-2 for external convective heat transfer coefficient; *eA* adaptive algorithm for external convective heat transfer coefficient; *eT* TARP for external convective heat transfer coefficient; *eM* MoWitt for external convective heat transfer coefficient

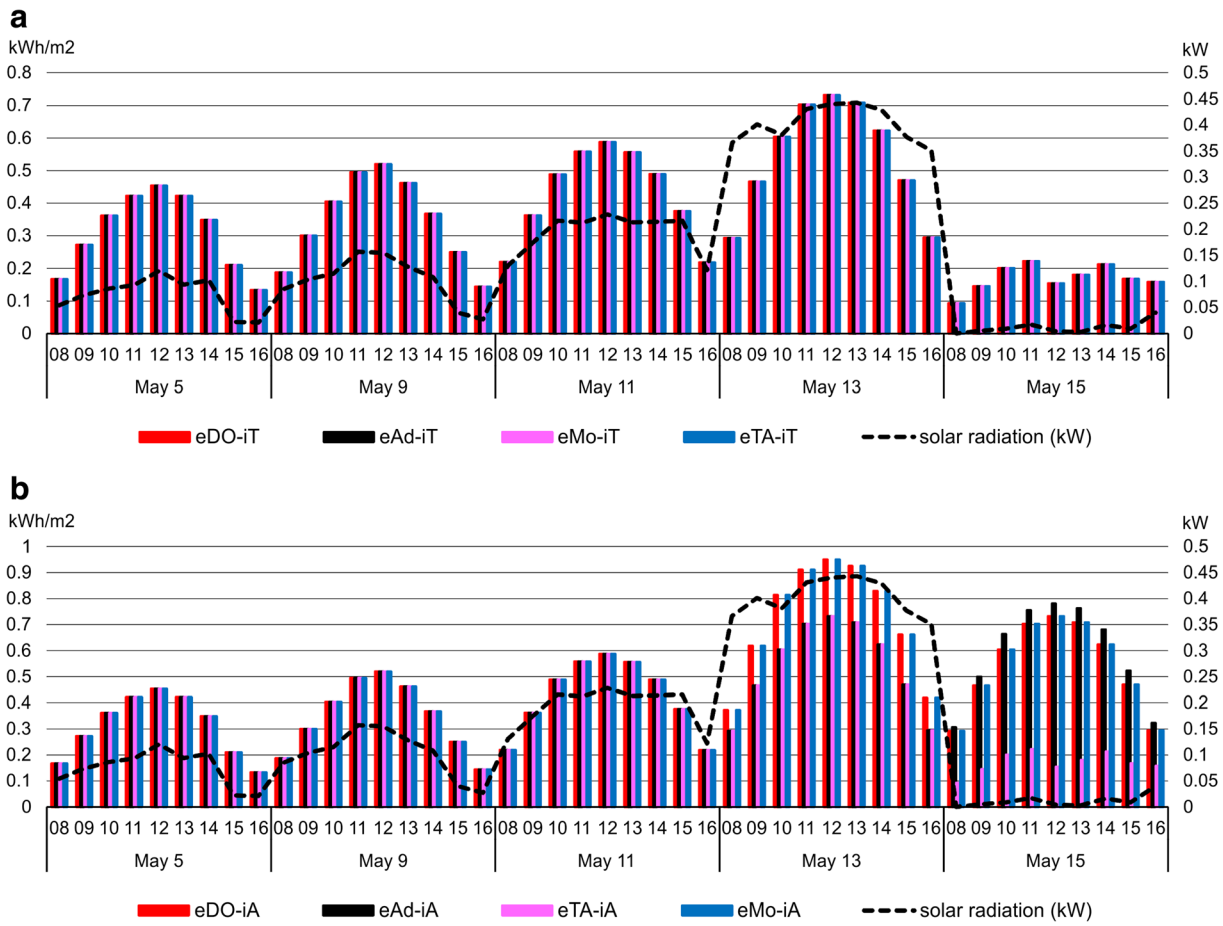


**Fig. 4** Solar radiation (kW/m$^2$), wind velocity (m/s), and solar gain (kW/m$^2$) calculations of the test building equipped with AS1 using various ICHTC and ECHTC models (*eDO* DOE-2 ECHTC, *eAd* adaptive ECHTC, *eTA* TARP ECHTC, *iT* TARP ICHTC, *iA* Adaptive ICHTC)

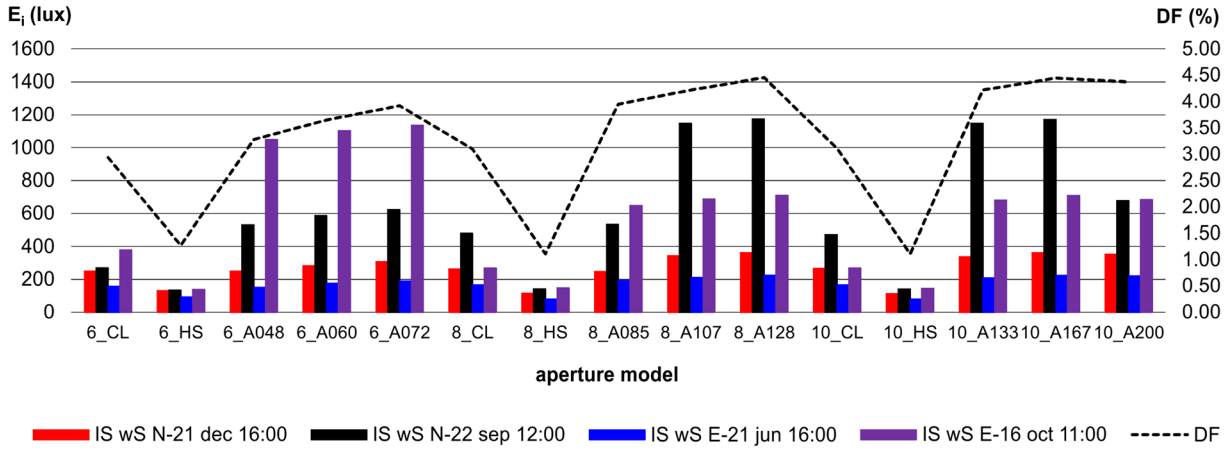


**Fig. 5** Average indoor illuminance (Lux) and DF (%) of building models equipped with various aperture models which are simulated using geographical position of Yogyakarta (*IS wS* intermediate sky with the sun; *N* north-facing aperture; *E* east-facing aperture)

## Daylight factors and the distributions

Radiance simulation results (Figs. 5 and 6) depict the daylighting performance superiority of AS. AS achieves the highest daylight levels (average DF and $E_i$ under the intermediate sky with the sun). All building models equipped with AS in Yogyakarta and Singapore have > 3% of DF and a similar pattern, although indoor illuminances of AS in Singapore are higher than those in Yogyakarta. If the simulation results are calibrated using the validation results in Table 3, the daylight levels of models equipped with AS are still higher than those of models equipped with a conventional aperture.

In terms of the daylight level, models equipped with clerestory only (CL) also perform well since the DF can reach 3% and the $E_i$ at low-altitude sun are slightly lower than the indoor illuminance of AS. Furthermore, the $E_i$ of all models equipped with CL in Singapore can reach 200 Lux. AS can increase the $E_i$ under intermediate sky with the low-altitude sun. In Yogyakarta, wider AS performs better when they are oriented to the North and narrower AS performs better when they are oriented to the East. While in Singapore, east-facing AS performs better than south-facing AS.

Daylight levels described in Figs. 5 and 6 demonstrate interesting results. Daylight levels of models equipped with CL and with SH remain the same, although the room width and the aperture size changes. However, the WFR of these models is 9.5%. This indicates that WFR rules of thumb can be applied to estimate the DF of conventional apertures, but cannot be applied for AS. In models equipped with AS, daylight

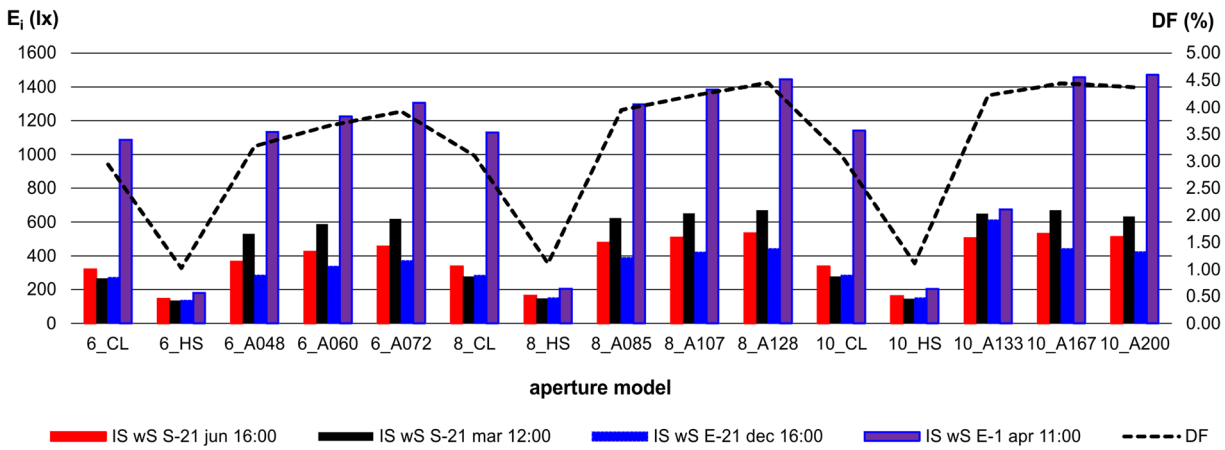


**Fig. 6** Average indoor illuminance (Lux) and DF (%) of building models equipped with various aperture models which are simulated using geographical position of Singapore (*IS wS* intermediate sky with the sun; *E* east-facing aperture; *S* south-facing aperture)

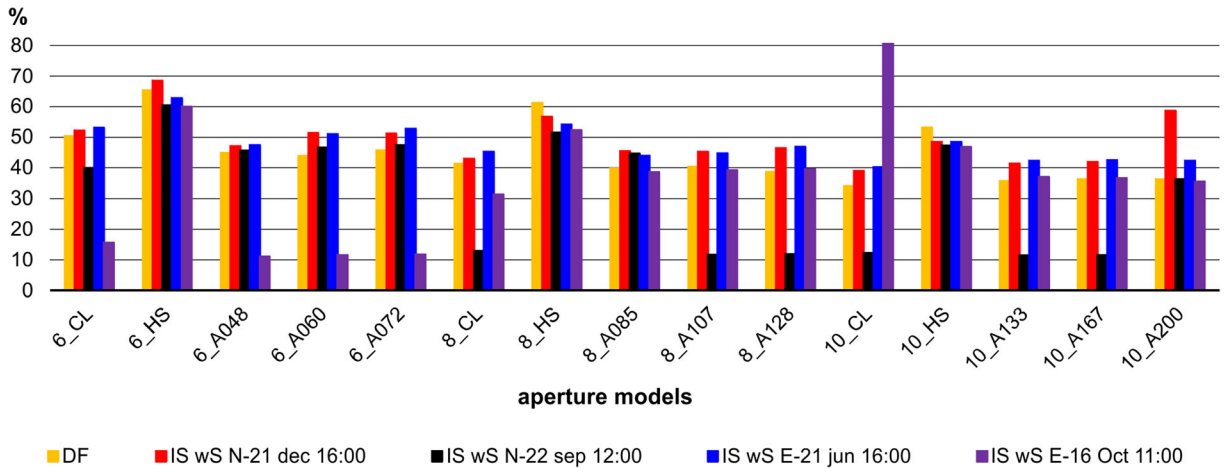


**Fig. 7** Indoor illuminance distributions (%) of building models equipped with various aperture, which are simulated using geographical position of Yogyakarta (*IS wS* intermediate sky with the sun; *N* north-facing aperture; *E* east-facing aperture; *S* south-facing aperture)

levels increase as the collector width rises. The angle spread of the anidolic collector coupled with the collector width determines the average DF and indoor illuminance.

However, the daylight distributions of AS only reach < 50% in Yogyakarta and < 55% in Singapore, although they are better than those of models with CL. The distributions drop when the collector angle spread cannot avoid direct sunlight as shown in Figs. 7 and 8 when the high-altitude sun on September 22 at 12:00 fell on north-facing collectors with ID: 8_A107, 8_A128, 10_A133, and 10_A167, and on October 16 at 11:00 fell on east-facing collectors with ID: 6_A108, 6_A060, and 6_A072 in Yogyakarta; and the high-altitude sun on April 1 at 11:00 fell on most of east-facing collectors, except collector 10_A133. Collectors 6_A048, 6_A060, and 6_A072 are suitable only for north-facing apertures in the southern hemisphere or south-facing apertures in the northern hemisphere. A high luminance sky in Singapore due to its proximity to the equator creates poor illuminance distribution for AS for east-facing apertures under sunlight (Fig. 8). Uneven indoor illuminance distributions (< 30%) occurred when the indoor illuminance is high (related to Figs. 5 and 6).

## The role of internal shelf in illuminance distribution

A light shelf can be installed to improve the indoor illuminance distributions (Binarti and Dewi 2016). In this study, the internal shelf width is the same as the

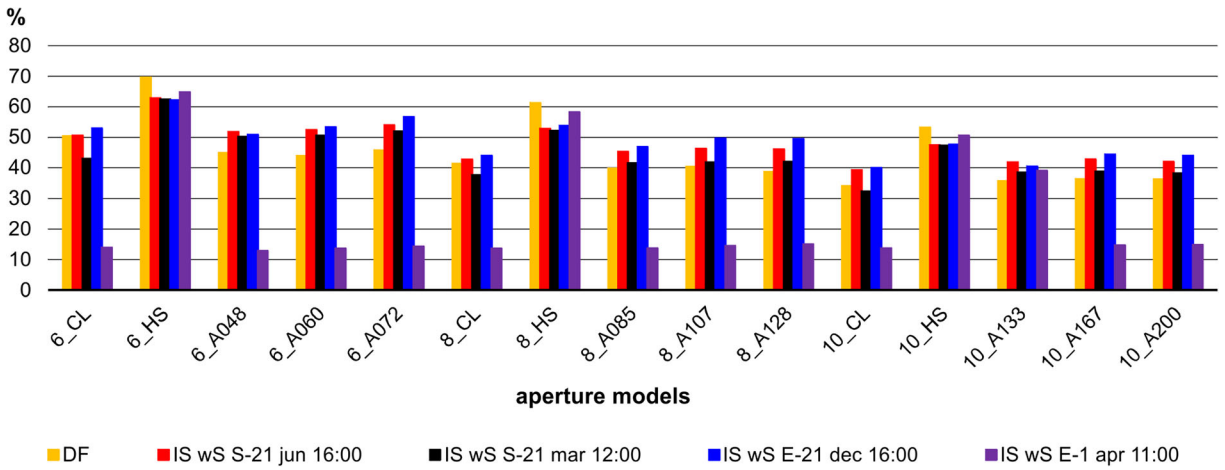


**Fig. 8** Indoor illuminance distributions (%) of building models equipped with various aperture, which are simulated using geographical position of Singapore (*IS wS* intermediate sky with the sun; *N* north-facing aperture; *E* east-facing aperture; *S* south-facing aperture)

**Table 7** Improvement in daylighting performance of modified AS compared to the daylighting performance of conventional apertures

| Aperture code | Avg $E_i$ (Lux) under intermediate sky with the sun 1 April at 11:00 | $E_i$ distribution (%) under intermediate sky with the sun 1 April at 11:00 | DF | |
|---|---|---|---|---|
| | | | Avg. value (%) | Distribution (%) |
| 6_CL | 1087 | 30.0 | 2.94 | 50.3 |
| 6_HS | 180 | 64.7 | 1.27 | 65.4 |
| 6_A048 | (1134) 508 | (26.7) 57.5 | (3.28) 2.18 | (44.8) 69.7 |
| 6_A060 | (1226) 576 | (25.7) 54.2 | (3.65) 2.43 | (43.8) 65.0 |
| 6_A072 | (1306) 630 | (27.1) 54.6 | (3.92) 2.61 | (45.7) 67.0 |
| 8_CL | 1130 | 25.5 | 3.10 | 41.3 |
| 8_HS | 206 | 53.4 | 1.11 | 61.3 |
| 8_A085 | (1297) 569 | (22.1) 48.9 | (3.95) 2.55 | (39.7) 59.2 |
| 8_A107 | (1385) 648 | (24.5) 46.8 | (4.22) 2.78 | (40.3) 57.6 |
| 8_A128 | (1445) 699 | (25.0) 47.8 | (4.45) 2.92 | (38.7) 59.9 |
| 10_CL | 1142 | 22.2 | 3.11 | 34.1 |
| 10_HS | 203 | 40.4 | 1.11 | 53.2 |
| 10_A133 | (674) 460 | (34.4) 48.5 | (4.22) 2.76 | (35.5) 51.4 |
| 10_A167 | (1457) 688 | (21.8) 40.3 | (4.44) 2.90 | (36.3) 51.0 |
| 10_A200 | (1470) 715 | (20.7) 41.7 | (4.37) 2.90 | (36.2) 50.7 |

Previous AS values are written inside the bracket

clerestory height with 3 cm for the additional width to prevent direct sunlight from around 9:00 a.m. until midday, especially for east-facing AS in Singapore under high sunlight. The results of the installation of internal shelves at 10 cm below the clerestory (Table 7) demonstrate significant improvements in the daylight (DF and indoor illuminance) distribution. The rising of the distribution ranges from 41 to 115% for the indoor illuminance distribution and from 40 to 56% for the DF. Although most of the values are still lower than the daylight distribution of horizontal-shading-equipped clerestories (HS), AS with internal shelves can achieve higher (more sufficient) indoor illuminance and DF. Collector 10_A133 with internal shelf is the only AS model that increases the daylight distribution more than the HS model. Adding a view window below the AS also can improve the horizontal illuminance distribution. Since a view window contributes to the daylight levels of the room, the size of the clerestory and collector can be reduced.

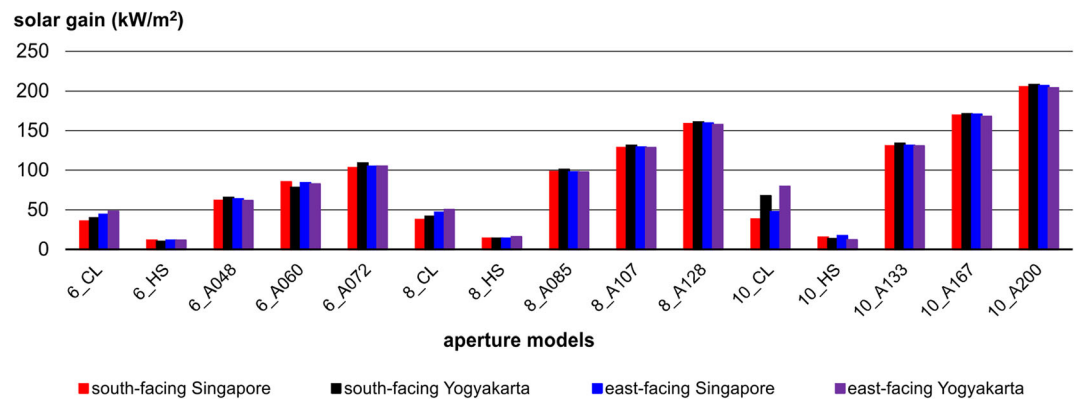


**Fig. 9** EnergyPlus simulations of the annual solar heat gain per floor area (kW/m$^2$) of an air conditioned building with various aperture models in Singapore and Yogyakarta

### Space solar gains and the impact on the indoor air temperature

Solar heat gain calculations for Yogyakarta and Singapore have similar patterns (Figs. 9 and 10). Zenithal-collector-glazing gains high solar radiation, which further creates higher space solar heat gains compared to buildings equipped with conventional apertures. The same position of the collector glazing (tilted 15°) creates similar annual solar heat gain per floor area for different aperture orientations (east- and south-facing). The wider the anidolic collector, the higher the annual space solar heat gain per floor area will be.

Compared to the building with clerestory only, the increase in the solar heat gain in Singapore is 73 to 190% for a 6-m-wide room with south-facing AS, 44 to 137% for a 6-m-wide room with east-facing AS, 162 to 324% for an 8-m-wide room with south-facing AS, 110 to 243% for an 8-m-wide room with east-facing AS, 242 to 437% for a 10-m-wide room with south-facing AS, and 175 to 334% for a 10-m-wide room with east-facing AS.

In higher latitudes (Yogyakarta), the increase in the solar heat gain due to the east-facing AS installation is less. The solar heat gain of the building equipped with AS increases from 64 to 175% for a 6-m-wide room with north-facing AS, −27 to 119% for a 6-m-wide room with east-facing AS, 142 to 286% for an 8-m-wide room with north-facing AS, 93 to 213% for an 8-m-wide room with east-facing AS, 99 to 209% for a 10-m-wide room with north-facing AS, and 65 to 158% for a 10-m-wide room with east-facing AS. The increase in the solar heat gain of AS-equipped buildings becomes much higher if they are compared to those of buildings with equipped horizontal shading.

Figure 10 illustrates the insignificant change of the indoor air temperature (< 1.5 °C) because of the different aperture model. For a room with a small aperture, modification in the aperture model will not alter the indoor air temperature substantially. However, since the increase in the solar heat gain potentially increases the building cooling load and the energy consumption, the dimension of AS should be defined by the minimum collector width and the clerestory height.

### Optimum collector size

Referring to the previous study on the AS daylighting performance (Binarti and Satwiko 2015), there should be an optimum collector and clerestory dimension that provides sufficient daylight level and gains low solar radiation. The next experiment explored how far the collector and clerestory dimension can achieve minimum (2%) DF with even distribution (≥ 60%) and low solar heat gains (close to the solar heat gain produced by HS). It focuses on east-facing collectors installed on an 8-m-wide room as the medium room width using Singapore weather data. Based on an assumption that space solar heat gains can be reduced by decreasing the aperture dimension, this study aims to obtain the smallest collector which still provides 2% of the DF with ≥ 60% of the illuminance distribution.

At first, the clerestory height was reduced to 75 cm and the collector width was varied with a constant angular spread (Table 8 no. 3). The results show that a narrower collector width produces lower daylight levels but better DF and indoor illuminance distribution. Reduction of the clerestory height decreases the DF and indoor illuminance to the minimum requirements, but improves the indoor illuminance distribution (C80_A128_w60 and

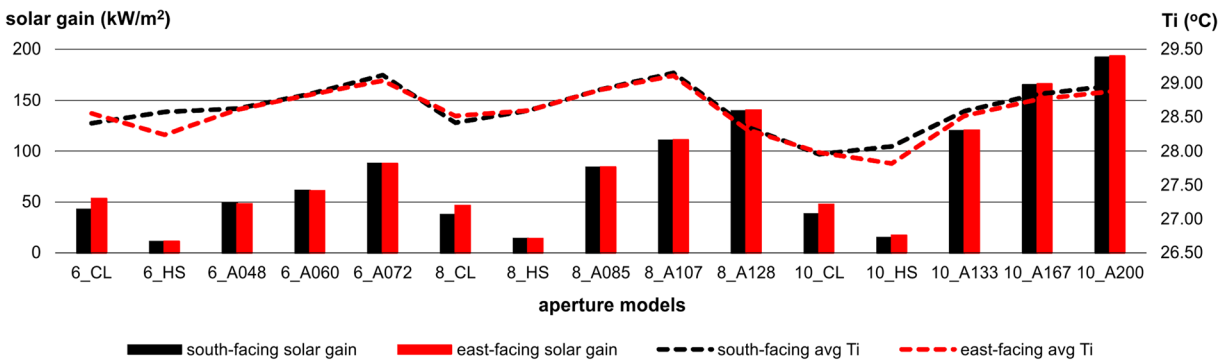


**Fig. 10** Annual solar heat gain per floor area and the indoor air temperatures of a naturally ventilated building with various aperture models in Singapore

C75_A128_w60). Although no AS can reach > 60% of the indoor illuminance distribution, > 55% of indoor illuminance distribution is good enough for a room without a view window. Adding a view window can increase the daylight levels near the window, which further increases the indoor illuminance distribution.

In the second step, the angular spread was varied with a constant and narrow collector width (Table 8 no. 4). Angular spreads of 52° and 45° created the highest DF and generally performed the best (highest indoor illuminance distribution with 2% of the DF. A smaller angular spread produces better daylight distribution with a lower daylight level. The next step is improving the daylight level of narrow (91-cm-wide) collectors with small angular spread (45° in no. 5 and 43° in no. 6) and increasing the clerestory height. The purpose of variation in clerestory height is to observe how far clerestory height improves the daylight levels and the distribution. The results in Table 8 no. 5 and 6 show that a narrow collector with small angular spread can achieve the same daylighting performance as that created by wider or bigger angular spread collectors.

Does the clerestory height of the same collector dimension increase the space solar heat gain significantly? To answer this question, the impact of different clerestory height and collector angular spread on the solar gain and indoor air temperature were studied. The overall result in Fig. 11 describes only insignificant effects on the indoor air temperature due to the variant collector size and the clerestory height.

Figure 11 also illustrates the impact of clerestory height, collector width, and angular spread applied on 8-m-wide, 3.2-m-high room (R8H3.2) on the annual space solar heat gains per floor area for air-conditioned buildings and the indoor air temperature (for naturally ventilated buildings) in Singapore. Results of models C75_A091_w60, C75_A108_w60, C75_A118_w60, and C75_A128_w60 demonstrate that increasing the collector width significantly affects the increase in the space solar gain. However, insignificant modification in the space solar gain appears

**Table 8** Daylighting performance of buildings equipped with east-facing AS with variations in collector width, angular spread, and collector height under overcast sky (DF) and under intermediate sky with the sun on 1 April at 11:00 in Singapore (indoor illuminance: $E_i$) compared to those of buildings equipped with east-facing conventional apertures

| No. | Models | Avg. DF (%) | Distribution of DF (%) | Floor area percentage of min. 2% of DF (%) | Avg. $E_i$ (lx) | Distribution of $E_i$ (%) | Floor area percentage of min. 300 lx of $E_i$ (%) |
|---|---|---|---|---|---|---|---|
| 1. | C80_CL | 3.10 | 41.3 | 60.0 | 1130 | 25.5 | 92.2 |
| | C80_HS | 1.11 | 61.3 | 0.0 | 206 | 53.4 | 17.8 |
| 2. | C80_A085_w45 | 2.55 | 59.2 | 62.2 | 569 | 48.5 | 91.6 |
| | C80_A107_w55 | 2.78 | 57.6 | 70.6 | 648 | 46.8 | 97.8 |
| | C80_A128_w60 | 2.92 | 59.9 | 75.6 | 699 | 47.8 | 99.8 |
| 3. | C75_A091_w60 | 2.10 | 59.5 | 50.9 | 476 | 48.5 | 70.9 |
| | C75_A108_w60 | 2.24 | 61.2 | 55.3 | 503 | 54.3 | 77.2 |
| | C75_A118_w60 | 2.61 | 68.2 | 70.3 | 512 | 49.4 | 77.8 |
| | C75_A128_w60 | 2.79 | 58.4 | 71.2 | 668 | 53.3 | 98.4 |
| 4. | C75_A091_w60 | 2.10 | 59.5 | 50.9 | 476 | 48.5 | 70.9 |
| | C75_A091_w52 | 2.12 | 60.4 | 50.6 | 463 | 56.6 | 70.3 |
| | C75_A091_w45 | 2.06 | 62.6 | 48.1 | 448 | 56.5 | 67.2 |
| | C75_A091_w43 | 1.94 | 63.4 | 41.6 | 421 | 49.9 | 81.9 |
| 5. | C80_A091_w45 | 2.64 | 58.7 | 65.9 | 618 | 53.3 | 95.0 |
| | C75_A091_w45 | 2.06 | 62.6 | 48.1 | 448 | 56.5 | 67.2 |
| | C70_A091_w45 | 2.40 | 57.9 | 58.1 | 564 | 43.1 | 81.9 |
| 6. | C85_A091_w43 | 2.66 | 62.0 | 66.6 | 614 | 49.7 | 97.2 |
| | C80_A091_w43 | 2.52 | 60.3 | 62.8 | 588 | 35.0 | 93.1 |
| | C75_A091_w43 | 1.98 | 61.6 | 43.8 | 427 | 48.7 | 64.7 |
| | C70_A091_w43 | 2.22 | 57.2 | 53.4 | 531 | 45.2 | 79.4 |

*R* room width, *H* room height in m, *C* collector height in cm, *A* collector width in cm, *w* collector angular spread in degree

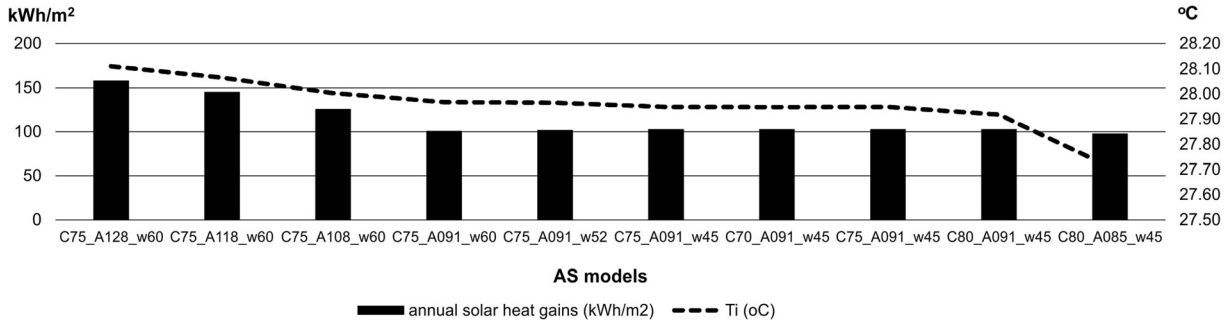


**Fig. 11** Annual solar heat gain per floor area (air conditioned buildings) and indoor air temperature (naturally ventilated buildings) of 8-m-wide, 3.2-m-high room equipped with various AS in Singapore (*C* collector height in cm, *A* collector width in cm, *w* collector angular spread in degree)

due to the decrease in the collector's angular spread (C75_A091_w60, C75_A091_w52, C75_A091_w45).

Results of models C80_A091_w45, C75_A091_w45, and C70_A091_w45 indicate that modification of clerestory height has no substantial impact on the annual space solar heat gain per floor area. Therefore, maximizing the clerestory height is suggested since it yields more even indoor illuminance distribution and improves the levels without increasing the solar heat gain. The medium angular spread of the collector (around 45°–52°) can be the optimum size to produce sufficient daylight levels (> 2% of the DF), even daylight distribution (> 55%), and relatively low solar heat gain or indoor air temperature.

## Conclusions

By comparing the daylighting and thermal performance of three apertures in Yogyakarta and Singapore, the energy saving potential of Anidolic System in the tropics have been assessed. Some critical points of the design of energy-saving anidolic system in the tropics are the following:

- Compared to the daylight levels of clerestory without shading and clerestory with horizontal shading, Anidolic System (AS) shows the superiority in achieving high daylight levels, both under the overcast and intermediate sky with the sun.
- The uneven indoor daylight level distribution (< 50%) can be improved by adding internal shelf with the average improvements of 95% for the indoor illuminance distribution and 47% for the daylight factor. The minimum width of an internal shelf or an interior panel below the clerestory is 10 cm more than the clerestory height in order to block direct sunlight during daytime. Adding a view window is another method to reach even indoor daylight level distribution that can be studied in detail in the future. Aperture with high daylight levels and even horizontal distribution has a great energy saving in lighting.
- In Yogyakarta, the width and the orientation of the AS collector are interdependent in determining the daylighting performance. Whereas, in Singapore north-facing collector produces lower (but more than sufficient) daylight levels with more even illuminance distribution than those of east-facing AS.
- Since anidolic collector captures high direct and diffuse solar radiation that contributes to space solar heat gain, wide collector should be avoided. Narrow anidolic collectors with maximum clerestory height can be the optimum AS to provide sufficient daylighting performance (DF ≥ 2%) with relative low solar heat gain. Collector with medium angular spread (45°–52°) produces a better daylight distribution (> 57%) than other angular spread and admits lower solar heat gain.
- Collector orientation insignificantly modifies the solar heat gain.

**Acknowledgements** Authors gratefully acknowledge the Directorate of Higher Education Republic Indonesia, Ministry of Research, Technology and Higher Education in the scheme of *Hibah Bersaing* (the second year) under the contract number 005/HB-LIT/III/2015 (Government to University) for supporting this study.

**Compliance with ethical standards**

**Conflict of interest** The authors declare that they have no conflict of interest.

## Appendix

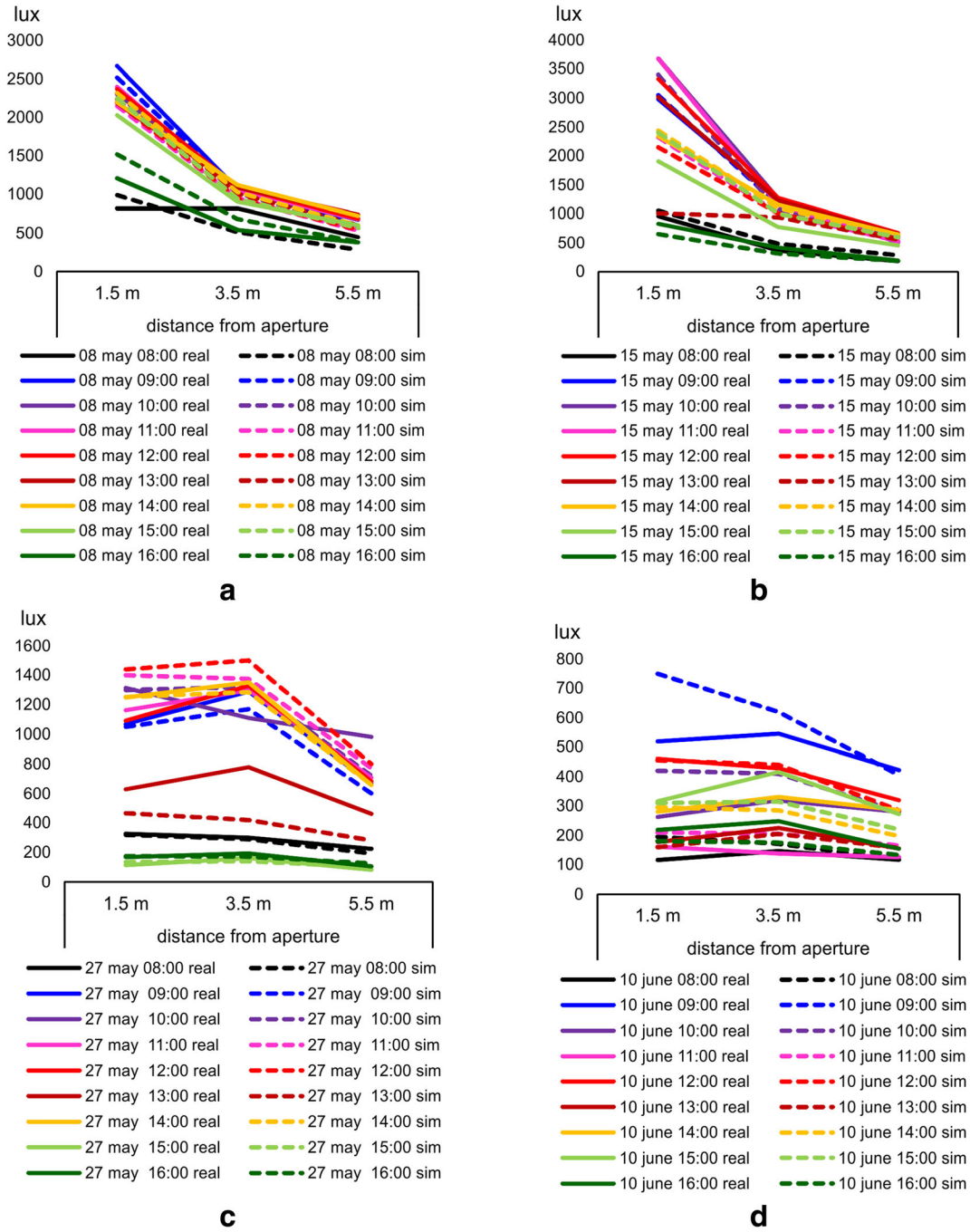


**Fig. 12** Field measured and simulated indoor illuminances of base model (equipped with clerestory only) (**a** and **b**), model with AS1 (**c**), and model with AS2 (**d**)

## References


Aizlewood, M. E. (1993). Innovative daylighting systems: an experimental evaluation. *Lighting Research and Technology, 25*(4), 141–152.

Al-Obaidi, K. M., Ismail, M., & Abdul Rahman, A. M. (2014). A study of the impacts of environmental loads that penetrate a passive skylight roofing system in Malaysian buildings. *Frontiers Architectural Research, 3*, 178–191.

ASHRAE. (2013). *ASHRAE Handbook: Fundamental*. Atlanta: ASHRAE.

Binarti, F. (2009). Energy-Efficient Window for Classroom in Warm Tropical Area. *11th International IBPSA Conference*, Glasgow, Scotland, UK, July 27–30, 2009, pp.1655–1662.

Binarti, F., & Dewi, S. (2016). The effectiveness of light shelf in tropical urban context. *Environmental and Climate Technologies December, 18*, 42–53. https://doi.org/10.1515/rtuect-2016-0012.

Binarti, F., & Satwiko, P. (2015). Long-term monitoring and simulations of the daylighting and thermal performance of an anidolic daylighting system on a tropical urban house. *Energy Procedia, 78*, 1787–1792. https://doi.org/10.1016/j.egypro.2015.11.307.

Binarti, F., & Satwiko, P. (2016). An east-facing anidolic daylighting system on a tropical urban house. *Indoor and Built Environment, 25*(4), 691–702. https://doi.org/10.1177/1420326X15574787.

Chirarattananon, S., & Chaiwiwatworakul, P. (2007). Distribution of sky luminance and radiance of North Bangkok under standard distributions. *Renewable Energy, 26*, 1328–1345.

Crawley, D.B., Lawrie, L.K., Winkelmann, F.C., Buhl, W.F., Pedersen, C.O., Strand, R.K., Liesen, R.J., Fisher, D.E., Witte, M.J., Henninger, R.H., Glazer, J., & Shirey, D. (2013). EnergyPlus v.8.1. Atlanta, Georgia.

Ellis, P. G. (2003). *Development and validation of the unvented Trombe Wall model in EnergyPlus*. USA: Master Thesis. University of Illinois at Urbana-Champaign.

Erell, E., Kaftan, E., & Garb, Y. (2014). Daylighting for Visual Comfort and Energy Conservation in Offices in Sunny Regions. Proc. of *30th International PLEA Conference - Sustainable Habitat for Developing Societies*, Ahmedabad, India, 16–18 December 2014.

Goia, F. (2016). Search for the optimal window-to-wall ratio in office buildings in different European climates and the implication on total energy saving potential. *Applied Energy, 132*, 467–492.

Hachem, C., Athienitis, A., & Fazio, P. (2011). Parametric investigation form effects on solar potential of housing units. *Solar Energy, 85*, 1864–1877.

Huang, Y., Niu, J.-L., & Chung, T.-M. (2014). Comprehensive analysis on thermal and daylighting performance of glazing and shading designs on office building envelope in cooling-dominant climates. *Applied Energy, 134*, 215–228.

Kleindienst, S.A. (2006). *Improving the daylighting conditions of existing buildings: the benefits and limitations of integrating anidolic daylighting systems using the American classroom as a model*. Master thesis, Massachusetts Institute of Technology, USA, 2006.

Leadership in Energy and Environmental Design (LEED). (2009). *Reference Guide for Green Building Design and Construction, for the Design, Construction and Major Renovations of Commercial and Institutional Building Including Core and Shell K-12 School Projects*, ed.www.usgbc.org. Accessed 6 November 2010.

Linhart, F., Wittkopf, S. K., & Scartezzini, J.-L. (2010). Performance of anidolic daylighting systems in tropical climates, parametric studies for identification of main influencing factors. *Solar Energy, 84*, 1085–1094.

Loutsenhiser, P. G., Manz, H., Felsmann, C., Strachan, P. A., Frank, T., & Maxwell, G. M. (2007). Empirical validation of models to compute solar irradiance on inclined surfaces for building energy simulation. *Solar Energy, 81*, 254–267.

Loutsenhiser, P. G., Manz, H., Carl, S., Simmler, H., & Maxwell, G. M. (2008). Empirical validations of solar gain models for a glazing unit with exterior and interior blind assemblies. *Energy and Buildings, 40*, 330–340.

Marsch, A.(2005). Ecotect Software v.5.5. Square One, Cardiff.

McNeil, A. & Lee, E. (2012). A validation of the Radiance three phase simulation method for modeling annual daylight performance of optically complex fenestration systems. *Building Performance Simulation* 1–14. DOI:https://doi.org/10.1080/19401493.2012.671852.

Michael, A., & Heracleous, C. (2016). Assessment of natural lighting performance and visual comfort of educational architecture in southern Europe: the case of typical educational school premises in Cyprus. *Energy and Buildings, 140*, 443–457.

Michael, A., Gregoriou, S., & Kalogirou, S. A. (2017). Environmental assessment of an integrated adaptive system for the improvement of indoor visual comfort of existing buildings. *Renewable Energy, 2017*. https://doi.org/10.1016/j.renene.2017.07.079.

Mirsadeghi, M., Costola, D., Blocken, B., & Hensen, J. L. M. (2013). Review of external convective heat transfer coefficient models in building energy simulation programs: implementation and uncertainty. *Applied Thermal Engineering, 56*(1–2), 134–151.

Praditwattanakit, R., Chaiwiwatworakul, P., & Chirarattananon, S. (2013). Anidolic concentrator to enhance the daylight use in tropical buildings. In: *International Conference on Alternative Energy in Developing Countries and Emerging Economies*. Bangkok, Thailand, 30–31 May 2013, ftp://202.28.64.61/04.April2013/Dowload/print/ 139_Rut%20Praditwattanakit.docx. Accessed 7 August 2014.

Prasetyo, S. S., & Kusumarini, Y. (2016). Studi Efisiensi dan Konservasi Energi pada Interior Gedung P Universitas Kristen Petra. *Jurnal INTRA, 4*(1), 36–45.

Pritchard, D.C. (ed). (1986). Interior lighting design, 6th ed., London: The Lighting Industry Federation Ltd. And The Electricity Council.

Rahim, R. & Mulyadi, R. (2004). Preliminary study of horizontal illuminance in Indonesia. In: *5th SENVAR*, Universiti Teknologi Malaysia, Skudai, Johor, Malaysia, 10–12 December 2004, pp.1–10.

Reinhart, C. F., & Andersen, M. (2006). Development and validation of a radiance model for a translucent panel. *Energy and Buildings, 38*(7), 890–904.

Roshan, M., Kandar, M. Z. B., Nikpur, M., Mohammadi, M. P., & Ghasemi, M. (2013). Investigating the performance of anidolic daylighting system with respect to building orientation in tropical area. *IRACST-ESTIJ, 3*, 74–79.

Scartezzini, J.-L., & Courret, G. (2002). Anidolic daylighting systems. *Solar Energy, 73*, 123–135.

Singh, R., Lazarus, I. J., & Kishore, V. V. N. (2015). Effect of internal woven roller shade and glazing on the energy and daylighting performances of an office building in the cold climate of Shillong. *Applied Energy, 159*, 317–333.

Standar Nasional Indonesia (SNI). (2011). *SNI-6390: Konservasi energi sistem tata udara bangunan gedung*. Jakarta: Badan Standardisasi Nasional.

Sunaga, N., Soebarto, V., Hyde, R., Ribeiro, M. A. Junghans, L., Binarti, F., & Calderaro, V. (2008). Chapter 9: design, elements, and strategies. In R. Hyde (Ed.), Bioclimatic housing: innovative designs for warm climates. London: Earthscan.

Tindale, A. & Potter, S. (2014). *DesignBuilder v.4.0*. Gloucestershire.

University of Illinois and Lawrence Berkeley National Laboratory. (2015). EnergyPlus Documentation: Engineering Reference.

Ward, G. (2002). *Desktop radiance software*. California: Lawrence Berkeley Laboratory.

Wittkopf, S. K. (2006). Daylight performance of anidolic ceiling under different sky conditions. *Solar Energy, 81*, 151–161.

Wittkopf, S. K., Grobe, L. O., Compagnon, R., Kampf, J., Linhart, F., & Scartezzini, J.-L. (2010). Ray tracing study for non-imaging daylight collectors. *Solar Energy, 84*, 986–996.

Zhu, D., Hong, T., Yan, D., & Wang, C. (2012). Comparison of building energy modeling programs: building loads. Ernest Orlando Lawrence Berkeley National Laboratory (LBNL) – 6034E. LA.